Composite Laminate Scarf-Repair Analysis: Software Implementation and Experimental Validation

*Sui-An Wang[1)], Zong-Hong Xie[2)] and Xiang Li[3)]

[1), 2), 3)] *School of Astronautics, Northwestern Polytechnical University, Xi'an 710072, China*

[1)] npuwangsuian@gmail.com

ABSTRACT

Existing analytical models were modified for the analysis of composite adhesively scarf-repaired joints subjected to unidirectional tension. Both analytical models for stepped-scarf repair joints and tapered-scarf repair joints were built, including the structures without extra plies, with one extra plies. The data structure and algorithm were developed and Accuracy Degree was defined to assess the accuracy of numerical calculation, implementing a user-friendly software program for the design and analysis of composite scarf repair under tensile load. The shear stress/strain distribution in the adhesive layer could be presented, the failure level of repair patch and the base laminate could be evaluated and the ultimate failure load can be predicted. T300/CYCOM-970 was used as adherent and METLBOND 1515-4M was used as adhesive. A series of corresponding experiments were conducted for validation. The results calculated by this software showed a good agreement with experiment outcomes that the relative errors for stepped-scarf repair are less than 5.7% and the relative errors for tapered-scarf repair are not more than 14.0%. This software provides an efficient and accurate preliminary design and analysis tool for the scarf repair of composite laminates.

1. INTRODUCTION

Due to the excellent specific strength, specific stiffness, fatigue properties, corrosion resistance, easy molding, and other outstanding overall performance, advanced composite materials has been widely used in the aviation, aerospace and other fields (Thoppul 2009, Banea 2009), which contributed to the development of composite structure damage assessment technique and repair technique. Composite structure repair techniques are generally be divided into mechanical connection technique and adhesive bonding technique. Compared with the mechanical connection technique, adhesive bonding technique has numerous advantages and has gradually been applied in the maintenance of civil aircraft structures (Wang 2016) .

Analytical approaches for adhesively bonded joints have been proposed by many researchers. The earliest study can be traced to Volkersen's viscous shear model, that

---

[1), 3)] Post-graduate student

[2)] Professor

posited only shear stress existed in the adhesive layer to simplify the solution process (Volkersen 1938). By extending Volkersen's works, Goland and Reissner considered the effect of bending moment at the end of adhesive layer, which not only caused the adherend's peeling stress, but also affected the distribution of shear stress (Goland 1944). Hart-Smith introduced the assumption of elastic-perfectly plastic adhesive, considering the effect of plastic deformation to adhesive film (Smith 1973). Yang and Pang applied Classical Laminated Plate Theory to analyze adhesively bonded joints, discussing the anti-symmetric structure and lateral shear deformation's influence on the joints (Yang 1993, Yang 1996). Recently, Zhang et al. proposed a method for multi-axial stress analysis of composite bonded joints, taking into account the effect of transverse shear and heat, and analyzing adherend's in-plane stress and inter-laminar stress (Zhang 2006). Liu et al. applied a semi-analytical method and FEA into the analysis of adhesively tapered-scarf joints (Liu 2015).

Ahn et al. adapted Hart-Smith's model to scarf and double sided lap repair by taking into account each individual layer separately (Ahn 1998). Based on Ahn's study, a modified method is presented in this paper, which includes the effect of the number of extra plies on the mechanical properties of the joints and an improved failure criterion for assessing adhesive. A repair tool, proposed in the present paper, is aimed to help designers analyze and design the adhesively bonded joints more efficiently.

2. ANALYTICAL MODEL

Composite adhesively bonded scarf repair technique can be generally divided into tapered-scarf repair joint and stepped-scarf repair joint (Fig. 1). The typical structure and geometrical properties of a scarf-repaired laminate are illustrated in Fig. 2. Here we define β as scarf angle, of which tangent is the ratio of the base laminate's (BL) thickness H and lap length d_s. Additionally, h_s is defined as step height. The smaller h_s is, the denser the total steps are, and stepped-scarf structure is closer to tapered-scarf structure. The correlation between h_s and taper-scarf structure is to be discussed in Section 1.2. The composite adhesively bonded joints can be always considered as "base laminate-adhesive layer-repair patch".

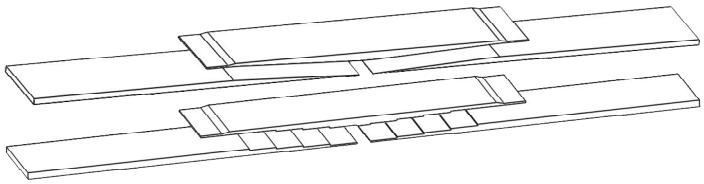

Fig. 1 Tapered scarf repair technique (upper) and stepped scarf repair technique (lower)

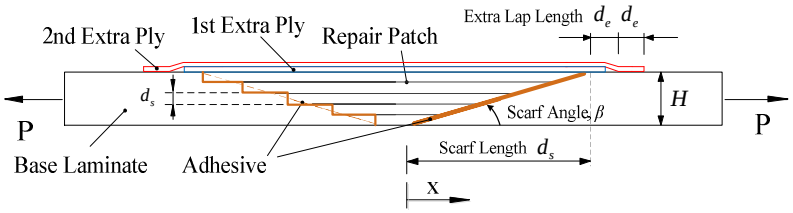

Fig. 2 Typical structure and geometry of a scarf-repaired joint

2.1 Model of stepped-repaired joint

2.1.1 Shear strain expression of adhesive

The model in the literature (Christensen 1998) only considered shear deformation along adhesive, without considering peeling stress in adhesive. Both the base laminate (BL) and the repair patch (RP) behaved in linearly elastic manner, while the adhesive layer exhibited elastic-perfectly plastic behavior (see Fig. 3). The shear strains at the elastic limit and at plastic failure are γ_{ef} and γ_{pf}, respectively. Based on the above assumptions and simplicity, the expressions for the shear strain in adhesive can be obtained.

In the elastic region, the shear stress expression for $i-th$ segment is

$$ {}^{i}\gamma_e(x) = {}^{i}\gamma = {}^{i}A\sinh({}^{i}\lambda x) + {}^{i}B\cosh({}^{i}\lambda x) \tag{1}$$

where $ {}^{i}\lambda = \sqrt{\frac{G}{h_a}\left({}^{i}a_{11}^{L} + {}^{i}a_{11}^{R}\right)}$

In the plastic region, the shear stress expression for $i-th$ segment is

$$ {}^{i}\gamma_p(x) = {}^{i}\gamma = \frac{({}^{i}\lambda)^2\gamma_{ef}}{2}x^2 + {}^{i}rx + {}^{i}s \tag{2}$$

Where $ {}^{i}a_{11}$ is the 11 component of the BL or RP compliance matrix in the $i-th$ segment; the right superscripts L and R refer to BL and RP; the left superscript i refers to $i-th$ segment; G is the shear modulus of the adhesive; h_a is the thickness of the adhesive. $ {}^{i}A, {}^{i}B, {}^{i}r$ and $ {}^{i}s$ in the Eqs.(1) and (2) are undermined constants which can be determined from the boundary and continuity conditions.

The shear strain expressions of all segments $ {}^{i}\gamma(x)$ (from 1 to K, K is the last segment) could be obtained under one given tensile load. By Hook's Law, it is easy to yield the shear strain expressions $ {}^{i}\tau(x)$. Then strain and stress in each segment of BL or RP can be achieved from force balances. Finally, the appropriate failure criteria are applied to assess the failure degree of the BL, the RP and the adhesive.

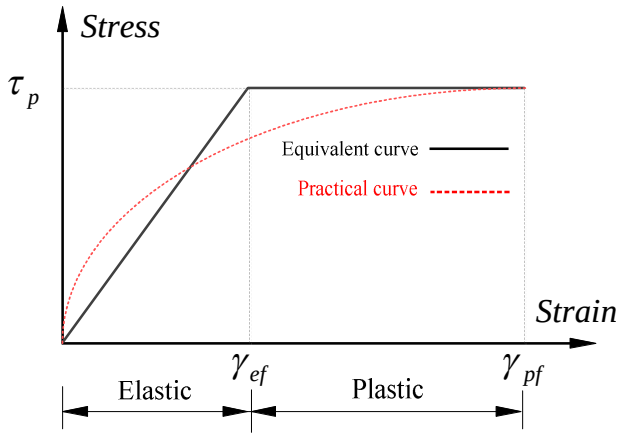

Fig. 3 The shear stress-strain relation of an elastic-perfect plastic adhesive

2.1.2 Boundary and continuity conditions

Analysis of the stepped-scarf structure can be simplified to that of a segment illustrated in Fig. 4. An $i-th$ segment consists of left plastic region, elastic region and right plastic region, of which the expressions are ${}^{i}\gamma_{p1}(x)$, ${}^{i}\gamma_{e}(x)$ and ${}^{i}\gamma_{p2}(x)$ respectively. Fig. 4 also presents the corresponding continuity conditions.

1) Boundary condition

The boundary conditions can be expressed as

$$\begin{cases} \dfrac{d({}^{1}\gamma)}{dx} = -\dfrac{P\times({}^{1}a_{11}^{R})}{h_a} & (x=0) \\ \dfrac{d({}^{K}\gamma)}{dx} = \dfrac{P\times({}^{K}a_{11}^{L})}{h_a} & (x=d_s) \end{cases} \tag{3}$$

2) Inter-segment continuity condition

It must be ensured that the shear strain in the adhesive is continuous and the in-plane loads are equal and opposite on the left and right sides of the segment. Accordingly, the continuity conditions at the edge of each segment are

$$\begin{aligned} {}^{i+1}\gamma &= {}^{i}\gamma \\ \frac{d({}^{i+1}\gamma)}{dx} &= \frac{d({}^{i}\gamma)}{dx}\left(\frac{{}^{i+1}a_{11}^{L}+{}^{i+1}a_{11}^{R}}{{}^{i}a_{11}^{L}+{}^{i}a_{11}^{R}}\right) \\ &\quad + \frac{P}{h_a}\left(\frac{{}^{i+1}a_{11}^{L}\,{}^{i}a_{11}^{R}-{}^{i}a_{11}^{L}\,{}^{i+1}a_{11}^{R}}{{}^{i}a_{11}^{L}+{}^{i}a_{11}^{R}}\right) \end{aligned} \tag{4}$$

3) Elastic-plastic continuity condition

At the locations where the elastic and plastic regions meet $({}^{i}x_{p1}, {}^{i}x_{p2})$, the shear strains in both regions should be equal and continuous

$$
\begin{aligned}
{}^{i}\gamma_e &= {}^{i}\gamma_p = (\gamma_{ef}) \\
\frac{d({}^{i}\gamma_e)}{dx} &= \frac{d({}^{i}\gamma_p)}{dx}
\end{aligned}
\tag{5}
$$

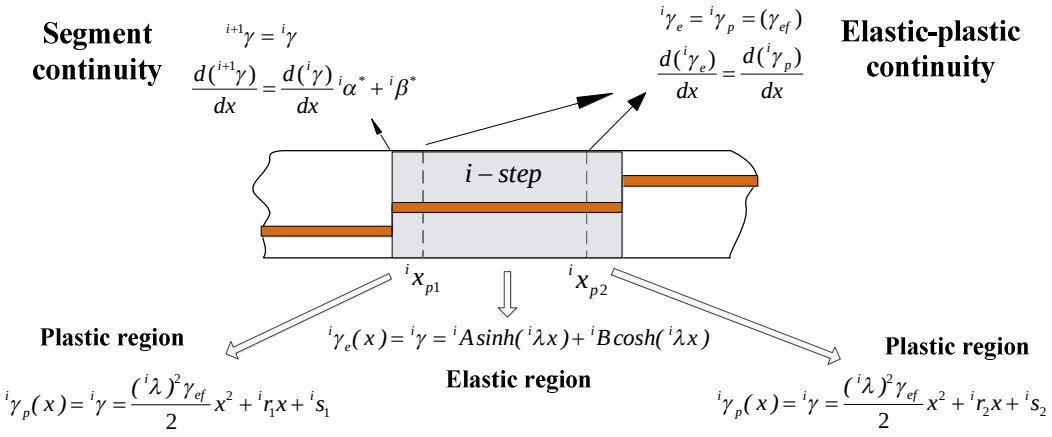

Fig. 4 Equations and continuity conditions for the $i-th$ segment

2.2 Model of tapered-repaired joint

An equivalent method is adopted to obtain the analytical model of the tapered-scarf structure. When increasing the numbers of total step of the stepped-scarf structure or reducing the value of h_s, the stepped-scarf structure is gradually approaching the tapered-scarf structure in appearance. The shear strain/stress field is the key property affects the reliability of the adhesive, thus we observe the change of the shear strain field to evaluate the rationality of this equivalent method.

The change of the shear strain and the maximum shear strain of the adhesive is demonstrated in Fig. 5, when h_s varies from 0.125mm (ply thickness of the BL or the RP) to 0.018mm. As can be seen, with the decrease of h_s, the shear strain field tend to converge into a unique field, and the maximum shear strain approach a specific value rapidly. The shear strain field is accurate enough once h_s is less than 0.03mm. However, there is no need to set h_s to too small value. Exorbitant step numbers may make the numerical errors ϕ (see 4.2) soar, resulting in erroneous results. So an optimum h_s should be determined to not only maintain the accuracy of tapered-scarf, but also guarantee calculating efficiency and numerical errors. Here, the stepped-scarf model with $h_s \le 0.03mm$ is used as the tapered-scarf model.

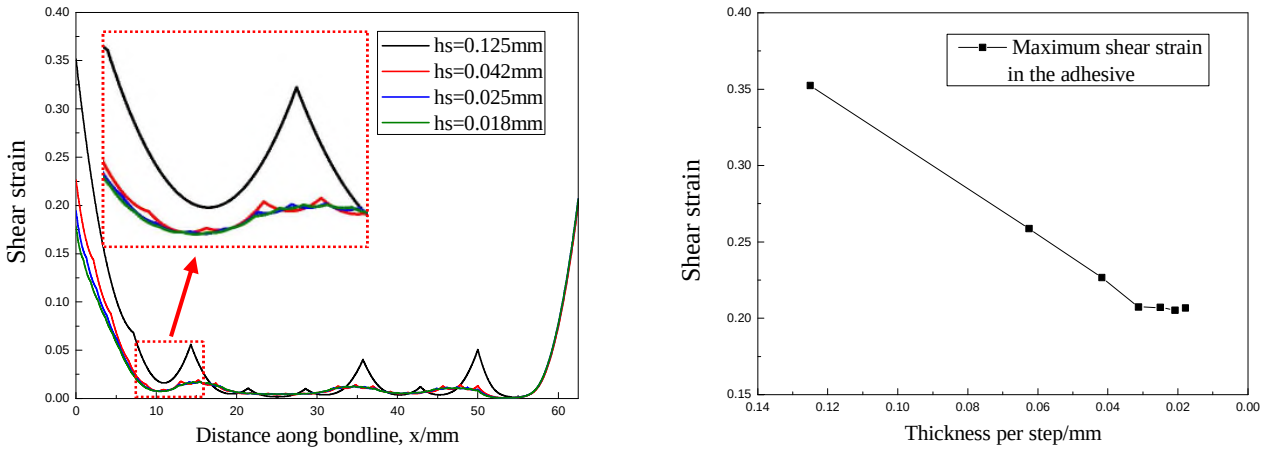

(a) Shear strain field (b) Maximum shear strain

Fig. 5 The change of shear strain field/maximum shear strain of the adhesive with h_s changing

3. FAILURE CRITERIA

Adhesively bonded joints may fail in the following modes independently or combined: (a) BL fracture; (b) RP fracture; (c) Adhesive Delamination. To predict the strength of the joints, the following failure criteria are introduced.

3.1 Criteria for composite laminate

Among the various failure criteria for composite laminate, Maximum Strain Failure Criterion is deemed to be one of the best criteria to examine failure. Failure is taken to occur when in any plies of the BL or RP meets the strain limit. The strain limit refers to the limited strain at the uniaxial stress state, which is able to be measured by experiment.

3.2 Criteria for adhesive

Failure of adhesive is generally determined by critical stress criteria or critical plastic strain criteria, that adhesive fails when the maximum shear stress or strain reach shear stress limit or shear strain limit.

But actually, damage occurring in a small region cannot lead to absolute failure of the whole adhesive. According to Damage Zone Theory, adhesive don't fail until the damaged area grows to a certain extent (Ban 2008). Here the damaged zone is modified as the damaged length, of which the shear strain exceeds the plastic shear strain limit. The range of the limited damaged length is validated by experiment.

For a certain adhesive, the total lap length is d_s, the damaged length is d_{pf}. Then failure indicator is defined as

$$D_R = \frac{d_{pf}}{d_s} \times 100\% \tag{6}$$

When $D_R > 5\%$, the adhesive is diagnosed to fail.

4. SOFTWARE IMPLEMENTATION

4.1 Algorithm

According to the literature (Ahn 1998), there are no more than two elastic-plastic transition points along the adhesive, which occurs at non-deterministic position. In fact, those points may occur simultaneously at all segments. As is shown in Fig. 8, there are a total of eight transition points. Therefore, an independent segment method is proposed, viewing per segment as an independent structure to be analyzed (Fig. 4). For all the segments, a series of elastic-plastic transition points are defined as ${}^{i}x_{p1}, {}^{i}x_{p2}$. The deformation modes of every segment of adhesive can be described by the value of ${}^{i}x_{p1}$ and ${}^{i}x_{p2}$. The adhesive of anyone segment generally contains a left plastic zone, an elastic zone and a right plastic zone (Fig. 4). On the basis of the above solving structure, the adhesive could be calculated by the following steps using equations, boundary and continuity conditions summarized in Section 2.

(a) Value of the adhesive shear strain at the first segment ${}^{1}\gamma$ (${}^{1}x = 0$) is assumed under an applied tensile load P. Combined with the known boundary condition $\left.\frac{d({}^{1}\gamma)}{dx}\right|_{{}^{1}x=0}$, the expression of the three zone ${}^{1}\gamma_{p1}(x)$, ${}^{1}\gamma_{e}(x)$ and ${}^{1}\gamma_{p2}(x)$ are obtained; The elastic-plastic transition points ${}^{1}x_{p1}$ and ${}^{1}x_{p2}$ are also achieved.

(b) With the expressions of the first segment and inter-segment continuity condition, it is easy to yield the boundary condition of the next segment, ${}^{2}\gamma|_{{}^{2}x=0}$ and $\left.\frac{d({}^{2}\gamma)}{dx}\right|_{{}^{2}x=0}$; Then the shear strain expressions of the second segment will be obtained.

(c) Repeat the procedure in step (b) until the last segment K and yield the right boundary condition $R = \left.\frac{d({}^{K}\gamma_{p2})}{dx}\right|_{x={}^{K}d_k - x_{p2}}$; The difference between R and the actual value of the boundary condition is defined as $\xi = \left| R - \frac{P \times ({}^{K}a_{11}^{L})}{h_a} \right|$.

(d) If ξ is less than the desired value, the calculating process ends up with accepting the initial assumption of ${}^{1}\gamma|_{{}^{1}x=0}$ and retaining the shear strain expressions. Otherwise, turn into step (e).

(e) Chang the assumption of the left boundary condition by ${}^{1}\gamma|_{{}^{1}x=0} + d\gamma \rightarrow {}^{1}\gamma|_{{}^{1}x=0}$ and

turn back to step (a). The value of $d\gamma$ is determined by the change of ξ. If ξ is getting smaller, it is reasonable to maintain it constant. But if ξ is getting larger, the sign of $d\gamma$ is considered to be wrong. So let $-d\gamma/2 \to d\gamma$, changing the direction of the loop. This optimization is so-called "Newton down-hill method"。

The shear strain expressions of the adhesive subjected to a certain load can be achieved through step (a) to (e). The above circulation is called inner-loop. Calculating the failure load needs another circulation, serving P as the control variable, which is called outer-loop. Newton down-hill method is again used to determine the value of the step size dP. It will find the desired P where the stress or strain distribution matches a specific failure criterion through the outer-loop.

4.2 Calculation accuracy

Due to the elastic-perfect plastic assumption of adhesive, the models have to be solved by numerical method indirectly, that will inevitably generate numerical errors. It may lead to the erroneous results once the errors are too large. Therefore, it is necessary to assess the accuracy of the calculation results, determining acceptable calculating error.

Theoretically, the applied tensile loading should always be equal to the integral of shear stress along the adhesive. Thus, the calculation accuracy can be described as the relative deviation of the values of them, namely ϕ is

$$\begin{aligned} \phi &= \frac{P^* - P}{P} \times 100\% \\ P^* &= \sum_{i=1}^{K} \int_0^{{}^i d_k} {}^i\tau(x)dx \end{aligned} \tag{7}$$

where P is the applied tensile loading; P^* is the integral shear stress along the adhesive ${}^i\tau(x)$.

When $|\phi| < 1\%$, the calculation outcomes are accurate enough to be accepted, according to experimental validation.

4.3 Software interfaces

Based on the above algorithm, a composite adhesively repair design and analysis system (*CARDAS*) was implemented. Fig. 6(a) shows the flow diagram of the software. The main interface of *CARDAS* is presented in Fig. 6(b), which contains four types of adhesively bonded repair techniques, including Stepped-scarf repair technique and tapered-scarf technique. The interface illustrated in Fig. 7 is the solving control panel, where user can choose to do the specific calculations and get the relative information. The shear strain/stress of adhesive could be plotted (see Fig. 8). Compared with FEA, *CARDAS* is more adaptable and efficient to do parametric analysis

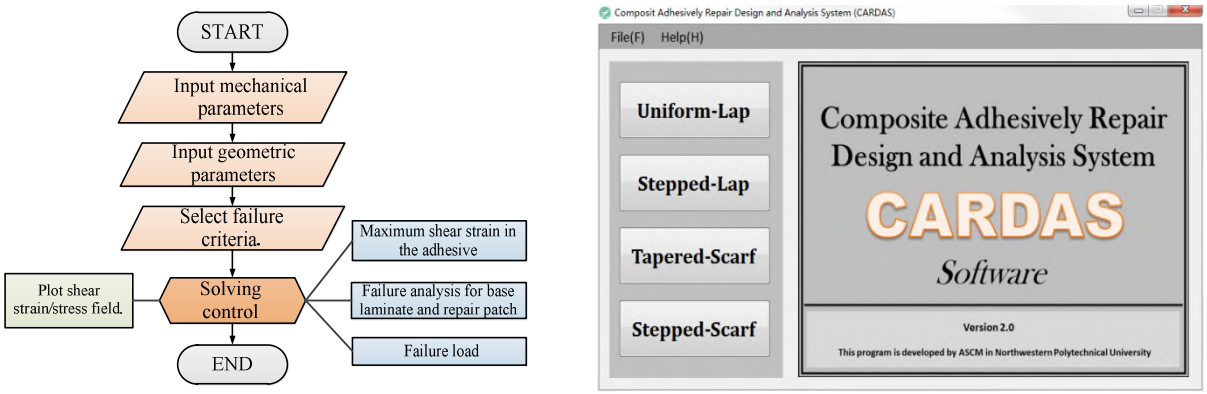

(a) Flow diagram (b) Main interface

Fig. 6 *CARDAS*'s flow diagram and main interface

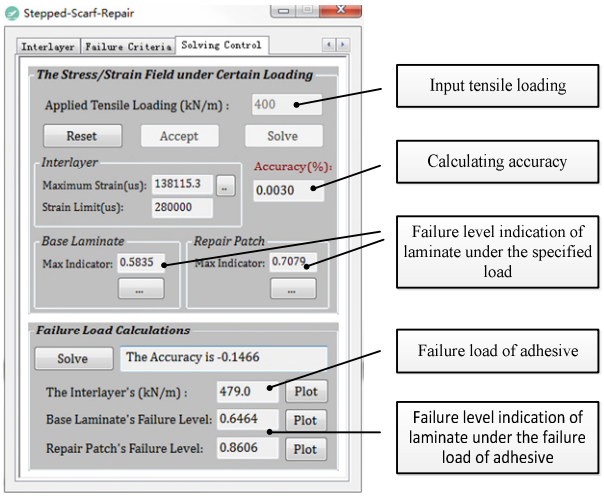

Fig. 7 Solving control interface

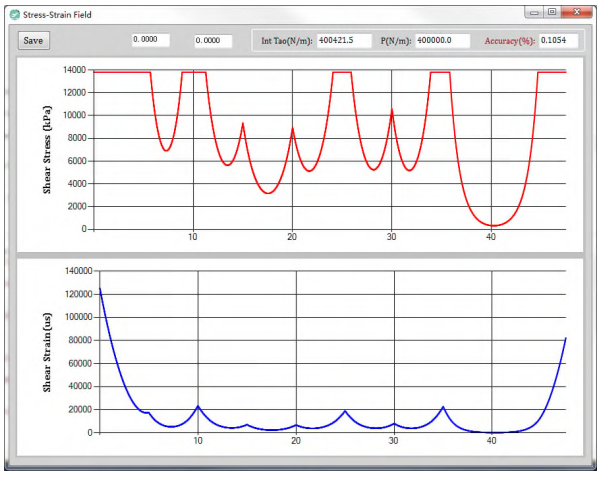

Fig. 8 Illustrating interface of shear strain/stress field

5. EXPERIMETN

5.1 Specimen materials

In this study, METLBOND 1515-4M, a stiff adhesive, were used as adhesives. T300/CYCOM 970, a fiber reinforced weave, were used as adherent. The materials above were all produced by Cytec. The BL was cured by auto-clave, while the RP was cured by hot-bonder. The mechanical properties of BL, RP and adhesive were tested in accordance with the ASTM standards, which are listed in Table 1 and 2.

Table 1 Mechanical properties of the laminates and the adhesive film

Mechanical properties	T300/CYCOM 970(Autoclave)	T300/CYCOM 970(Hot-bonder)	Metlbond 1515-4M
$E_1(GPa)$	66.5	59.1	3.57
$E_2(GPa)$	66.5	59.1	
$G_{12}(GPa)$	4.7	3.9	0.37
v_{12}	0.07	0.05	
$X_t(MPa)$	611.1	510.6	
$Y_t(MPa)$	611.1	510.6	
$S(MPa)$	121.3	113	
$\tau_p(MPa)$			13.8
γ_{pf}			0.30

Table 2 Geometrical properties of the materials

Geometrical properties	Base laminate	Repair patch	Extra plies	Adhesive
Ply sequences	$(0/45)_{2S}$	$(0/45)_{2S}$	$(0)_2$	
Ply numbers	8	8	1~2	
Ply thickness(mm)	0.210	0.210	0.205	0.125

5.2 Specimens and tests

Double-sided lap repair specimen: The lap length L_p of the four sets of specimens is 5mm, 15mm, 25mm and 35mm respectively. The width of all specimens is 25mm, of which other geometric parameters are shown in Fig. 9. The properties τ_p and γ_{pf} of the adhesive were hardly measured, therefore, double sided lap repair tests were implemented to deduce those two properties. The method is matching the

model to the four data points, to get optimum value of τ_p and γ_{pf}.

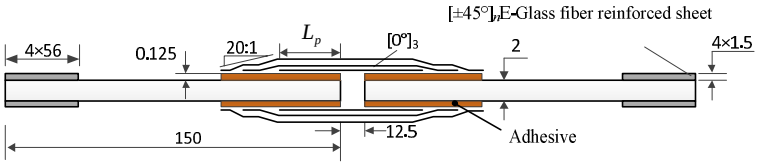

Fig. 9 Geometric parameters of adhesively double stepped-lap joints

Stepped-scarf repair specimens: The equivalent scarf angle is 3° and the total lap length is 40mm. The numbers of step are 2, 4, 8 (corresponding step lap length are 40mm, 13.4mm and 5.7mm) respectively. For 4-steps specimens, specimens with one extra ply and with two extra plies were added, of which per extra lap length is 12.5mm (Fig. 10).

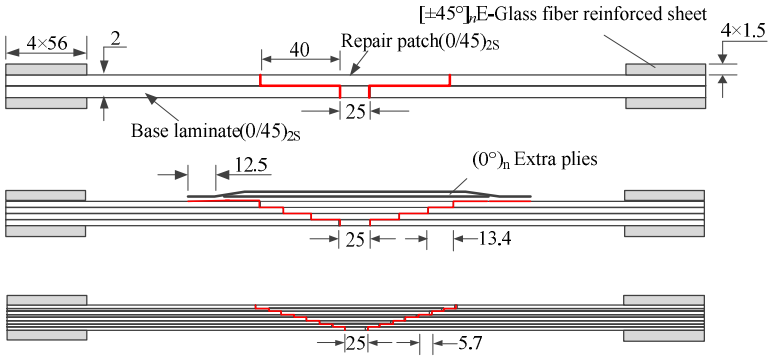

Fig. 10 Geometric parameters of adhesively stepped-scarf joints

Tapered-scarf repair specimens: In terms of numbers of extra plies, the specimens can be divided into specimens with one extra ply and specimens with two extra plies. The design scarf angle was $2^\circ, 3^\circ, 4^\circ, 5^\circ$ (actual scarf angles are listed in Table 4) respectively. Other geometrical parameters were shown in Fig. 11.

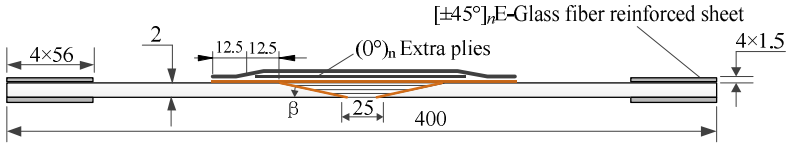

Fig. 11 Geometric parameters of adhesively tapered-scarf joints

An HUALONG DW-300 hydraulic pressure servo material testing machine was used for the tensile tests (Fig. 12). The load was applied at a constant head

displacement rate of 1mm/min up to ultimate failure of the specimens.

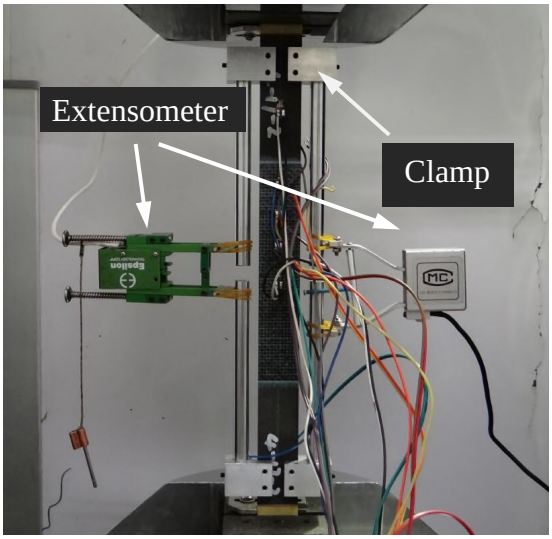

Fig. 12 Tensile testing setup of scarf-repaired specimen

6. EXPERIMETNTAL RESULTS AND DISCUSSION

6.1 Experimental results

Tensile test results of stepped-scarf repaired joints are listed in Table 3. Those measured data are stable and reliable, of which the coefficients of variation (CV) are pretty small (mostly below 5%). The strength recovery ratio of specimen without extra plies is 27.2%, 40.6% and 48.9% (specimen's strength/BL's strength) respectively. Every doubling the number of the steps can increase a 10.9% extra strength recovery on average. For specimens with 4 steps, the strength recovery ratio varies from 40.6%, 44.8% to 48.3%. One additional extra ply adds to an average 3.9% extra strength recovery. Increasing the number of step or extra ply can effectively reduce the edge stress concentration and improve stress distribution, to markedly enhance the strength of the joints.

Table 4 presents the tensile test results of tapered-scarf repaired joints, of which the CV is slightly larger than that of stepped-scarf joints' results. But the test data of tapered-scarf is still stable and reliable enough. The strength recovery ratio of the specimens ranges from 34.9% to 67.6%. The strength of tapered-scarf repair joints is negatively related to scarf angle in the range from 1.5 degree from 5 degree. Adding the number of extra ply has an obvious strength promotion to the joints. Under the same scarf angle, the joints with two extra plies obtain an average strength promotion of 44.7MPa (7.3%) than the joints with one extra ply.

Table 3 Tensile test results of stepped-scarf repaired joints

Specimen	Number of specimens	Number of steps	Number of extra plies	Strength (MPa)	
				Average	CV(%)
A1	3	2	0	166	0.6
A2	3	4	0	248	1.7
A3	3	4	1	274	3.8
A4	3	4	2	295	8.8
A5	3	8	0	299	1.6

Table 4 Tensile test results of tapered-scarf repaired joints

Specimen	Number of specimens	Scarf angle		Number of extra plies	Strength(MPa)	
		Design	Actual		Average	CV(%)
B1	3	2	1.75	1	406	4.3
B2	3			2	413	2.9
C1	3	3	2.63	1	342	5.6
C2	3			2	353	7.5
D1	3	4	3.50	1	263	7.5
D2	3			2	335	11.1
E1	3	5	4.38	1	213	8.1
E2	3			2	302	16.4

6.1 Discussion

The mechanical and geometrical parameters of those specimens and selected failure criteria were input into *CARDAS* to gain the corresponding calculation strength of the specimens. Stepped-scarf's comparison of experimental strength and calculation strength for the joints without extra ply is shown in Fig. 13(a). The calculation results are consistent with the experimental results (maximum relative error below 5.7%). Comparison for the joints with 4 steps is shown in Fig. 13(b). Those calculation results also show a good agreement with the experimental results. The relative errors are all less than 4.3%. As seen, the proposed software yields good prediction for all the stepped-scarf repair joints.

Fig. 14 shows the curves relating calculation strength to scarf angle for joints with one extra ply and with two extra plies, respectively. The experimental results are scattered on the corresponding figures for comparison. Those two calculated curves reflect the decreasing trend of joints' strength with scarf angle increasing. As seen, the experimental results are perfectly in accordance with the calculated curve for the joints with one extra ply (Fig. 14(a)). The relative errors at the four test points are all less than 4.5%, which are pretty small. By contrast, in Fig. 14(b) the experimental results for the joints with two extra plies don't agree so well with the corresponding calculated results

(maximum relative error 14.0%). The joints with two extra plies can achieve an increased calculation strength of 41.4MPa than the joints with one extra ply on average. The value is quite consistent with the experimental results (44.7MPa).

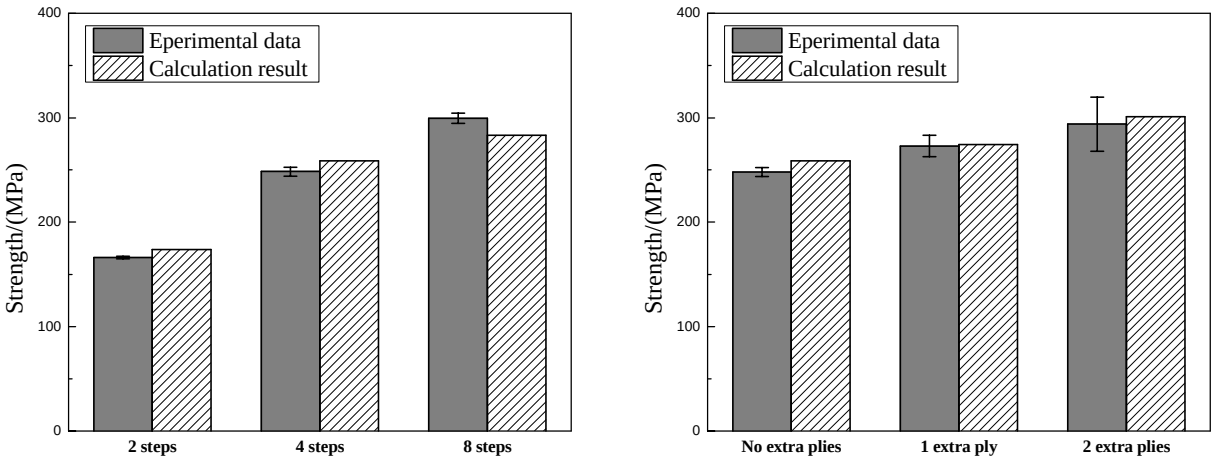

(a) With no extra plies (b) 4 steps

Fig. 13 Stepped-scarf's comparison of experimental strength and calculation strength

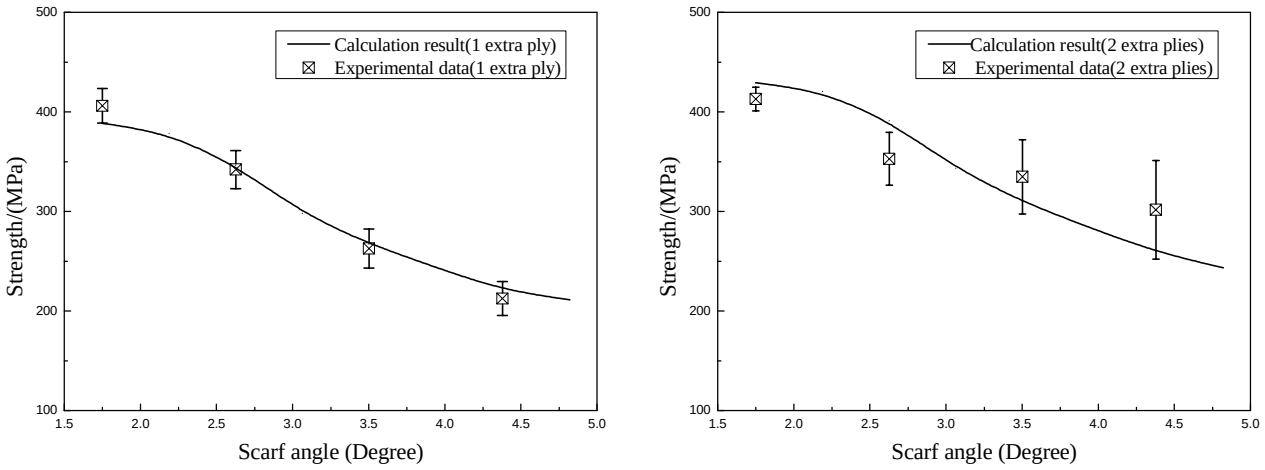

(a) With one extra ply (b) With two extra plies

Fig. 14 Tapered-scarf's comparison of experimental strength and calculation strength

7. CONCLUSIONS

In this study, the mechanical behaviors of four different types of stepped-scarf joints and eight different types of tapered-scarf joints subjected to tensile loading were investigated by analytical calculation and experimental validation. Accordingly, the

following conclusions can be drawn:

- Analytical model for stepped-scarf repair and tapered-scarf repair are presented. The corresponding data structure and algorithm for the analytical models are developed to implement the software *CARDAS*, which is helpful to do parametric analysis to adhesively bonded joints efficiently.
- According to the data obtained from the experiments, for the stepped-scarf joints having the same lap length, every doubling the number of the steps can increase a 10.9% extra strength recovery on average and one additional extra ply adds to an average 3.9% extra strength recovery.
- For the tapered-scarf joints having the same extra ply, the strength is negatively related to scarf angle in the range from 1.5 degree from 5 degree. The joints having the same scarf angle with two extra plies obtain an average strength promotion of 44.7MPa (7.3%) than that with one extra ply.
- Comparisons between experimental results and calculation results show a good agreement. For stepped-scarf joints, the maximum relative error is just 5.7%, while it is 14.0% for tapered-scarf joints. Accordingly, the proposed software *CARDAS* is a practical assistance tool for analysis and design of composite laminate adhesively bonded repair.

ACKNOWKEDGMENTS

The work is supported by the National Natural Science Foundation of China (Grant No. U1233202)

REFERENCES

Ahn S H, Springer G S. (1998), “Repair of Composite Laminates-II: Models.” Journal of Composite Materials, Vol. 32(11):1076-1114.

Ahn S H, Springer G S. (1998), “Repair of composite laminates-I: test results.” Journal of Composite Materials, Vol. 32(11):1036-1074.

Ban C S, Lee Y H, Choi J H, et al. (2008), “Strength prediction of adhesive joints using the modified damage zone theory.” Composite Structures, Vol. 86(1–3):96-100.

Banea M D, da Silva L F M. (2009), “Adhesively bonded joints in composite materials: an overview.” Proceedings of the Institution of Mechanical Engineers, Part L: Journal of Materials Design and Applications, Vol. 223(1): 1-18.

Bednarcyk B A, Zhang J, Collier C S, et al. (2006), “Analysis tools for adhesively bonded composite joints, part 1: higher-order theory.” AIAA journal, Vol. 44(1): 171-180.

Christensen, R. M, McCoy, J. J. (1970), *Mechanics of Composite Materials*, Pergamon Press.

Thoppul S D, Finegan J, Gibson R F. Mechanics of mechanically fastened joints in polymer–matrix composite structures–a review[J]. Composites Science and Technology, 2009, 69(3): 301-329.
WANG Yishou, QING Xinlin. Progress on study of structural health monitoring technology for composite joints. AMCS, 2016, 33(1): 1-16.
Goland M, Reissner E. (1944), “The stresses in cemented joints.” Journal of applied mechanics, Vol. 11(1): A17-A27.
Hart-Smith L J. (1973), *Adhesive-bonded single-lap joints*, Hampton, VA: Langley Research Center.
Liu B, Xu F, Ji Z, et al. (2015), “Modified semi-analytical method for adhesive stress of scarf joints in composite structure.” Acta Materiae Composite Sinica, Vol. 32(2):526-533
Volkersen O. (1938), “Rivet strength distribution in tensile-stressed rivet joints with constant cross-section.” Luftfahrforschung, Vol. 15(1): 41-47.
Yang C, Pang S S. (1993), “Stress-strain analysis of adhesive-bonded single-lap composite joints under cylindrical bending.” Composites Engineering, Vol.3(11): 1051-1063.
Yang C, Pang S S. (1996), “Stress-strain analysis of single-lap composite joints under tension.” Journal of Engineering Materials and Technology, Vol. 118(2): 247-255.
Zhang J, Bednarcyk B A, Collier C S, et al. (2006), “Analysis tools for adhesively bonded composite joints, part 2: unified analytical theory.” AIAA journal, Vol. 44(8): 1709-1719.